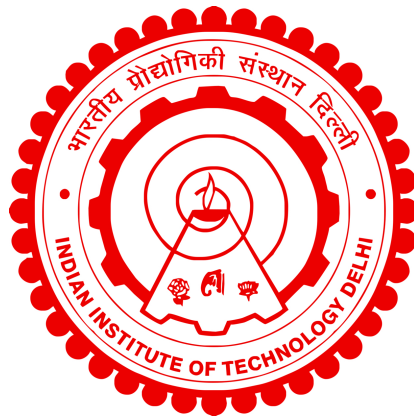


**POLARIZATION SINGULARITIES:
SYNTHESIS, CHARACTERIZATION AND
APPLICATION**

KAPIL KUMAR GANGWAR



DEPARTMENT OF PHYSICS

INDIAN INSTITUTE OF TECHNOLOGY DELHI

JULY 2025

© Indian Institute of Technology Delhi (IITD), New Delhi, 2025

Polarization Singularities: Synthesis, Characterization and Application

by

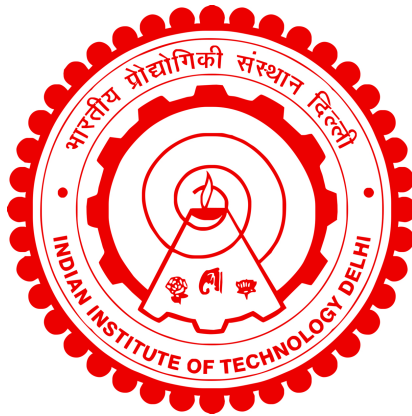
KAPIL KUMAR GANGWAR

Department of Physics

Submitted

in fulfilment of the requirements of the degree of Doctor of Philosophy

to the



**INDIAN INSTITUTE OF TECHNOLOGY
DELHI**

JULY 2025

Dedicated to my family

Certificate

This is to certify that the thesis entitled “**Polarization Singularities: Synthesis, Characterization and Application**”, submitted by **Kapil Kumar Gangwar** to the Indian Institute of Technology Delhi, for the award of the degree of **Doctor of Philosophy** in Department of Physics, is a record of the original, bona fide research work carried out by him under our supervision and guidance. The thesis has reached the standards fulfilling the requirements of the regulations related to the award of the degree.

The results contained in this thesis have not been submitted in part or in full to any other University or Institute for the award of any degree or diploma to the best of our knowledge.

Prof. P. Senthilkumaran
Optics and Photonics Centre,
Department of Physics,
Indian Institute of Technology Delhi.

Acknowledgements

I would like to express my sincere gratitude to my supervisor, Prof. P. Senthil Kumar, for his invaluable guidance, continuous support, and encouragement throughout this research journey. His profound expertise, keen insights, and patience in addressing my questions have played a pivotal role in shaping this work. His ability to foster independent thinking while providing constructive feedback has been truly inspiring. I am deeply grateful for the academic freedom and opportunities he has provided, which have allowed me to explore new ideas and grow as a researcher.

I extend my heartfelt thanks to the SRC members, including Prof. Joby Joseph, Prof. Sunil Kumar, and Prof. S. Aravindan for their valuable suggestions, critical insights, and constructive feedback during the progress of my research. Their expertise and guidance have significantly contributed to the quality and depth of this thesis. Their thoughtful discussions have helped refine my work, pushing me to consider broader perspectives and improve my approach.

I am also immensely grateful to the Indian Institute of Technology Delhi (IIT Delhi) for providing an excellent research environment, world-class facilities, and a stimulating intellectual atmosphere that have been crucial in carrying out this research. Additionally, I sincerely appreciate the financial support from the Department of Science and Technology—Science and Engineering Research Board (DST-SERB), which made this work possible by enabling access to essential resources and research opportunities.

A special note of appreciation goes to my lab seniors: Dr. Deepa, Dr. Sushanta Kumar Pal, Dr. Ruchi, Dr. Gauri, Dr. Manisha, and Dr. Baby Komal, with particular thanks to Dr. Sarvesh Bansal, who has been not only an invaluable mentor and guide but also my best friend throughout this journey. His constant support, insightful discussions, and encouragement have been instrumental in navigating various research challenges. His friendship has provided unwavering motivation, making even the most difficult times manageable.

I am equally grateful to my labmates, Anuj Maurya, Rahul Joshi, Sawpneel Chitriv, Susheel Bhardwaj and Mohammad Umar, who have been an integral part of this journey. Their camaraderie, collaborative spirit, and stimulating discussions have

fostered an engaging and supportive research environment. The countless hours spent brainstorming ideas, troubleshooting experiments, and exchanging knowledge have been invaluable. Their enthusiasm and friendship have made this research journey both intellectually rewarding and personally fulfilling.

A very special acknowledgement goes to my wife, Priya Gangwar, for her unconditional love, unwavering support, patience, and encouragement throughout this journey. Her belief in me, constant motivation, and sacrifices have been the foundation of my strength, and I am deeply grateful for her presence in my life.

Finally, I would like to extend my deepest appreciation to my family and friends for their unwavering support and encouragement throughout this journey. My family's unconditional love and sacrifices have given me the resilience to pursue my academic goals, and my friends' unwavering support has provided much-needed moments of relief, laughter, and inspiration.

This research would not have been possible without the collective contributions of all these individuals, to whom I am truly indebted.

Kapil Kumar Gangwar

Abstract

This thesis explores the generation, manipulation, and characterization of polarization singularities in structured light fields using innovative optical techniques. Polarization singularities, such as C-points and V-points, are topological features of vector beams that hold immense potential in singular optics. The work presented here is centered on developing efficient, controllable methods for creating singular beams, analyzing their properties, and studying their behavior under various conditions.

Novel strategies, including the use of Dammann gratings and phase ramps via spatial light modulators, are implemented to generate polarization singularity lattices with tunable indices and handedness. Composite polarization vortices are realized using a common-path polarization interferometer. This composite vortex is surrounded by C-point rings, and their properties are investigated through Stokes field analysis. Furthermore, a robust interference-based approach is proposed to identify and resolve degeneracy in the index. By finding spin and orbital angular momentum components, the degeneracy is lifted. The analysis of interference fringes with a tilted reference beam enables direct determination of the Stokes indices.

Furthermore, the effect of optical aberrations—specifically astigmatism—is investigated both theoretically and experimentally. By analyzing the transformation of intensity profiles under varying astigmatic strengths, the study demonstrates a quantifiable relationship between the aberration and the singularity structure. This provides a new method for characterizing both polarization singularities and lens aberrations, with implications in optical metrology and adaptive optics.

Theoretical predictions are consistently validated through detailed simulations and precise experiments, highlighting the practicality and accuracy of the proposed techniques. The findings have important implications for optical metrology, beam diagnostics, adaptive optics, and applications in optical trapping and free-space communication systems.

सार

यह शोध संरचित प्रकाश क्षेत्रों में ध्रुवण विषमताओं की उत्पत्ति, नियंत्रण और विशेषता निर्धारण की खोज करता है, जिसमें नवीन प्रकाशीय तकनीकों का उपयोग किया गया है। ध्रुवण विषमताएँ, जैसे कि सी-बिंदु और वी-बिंदु, सदिश प्रकाश किरणों की रूपात्मक विशेषताएँ होती हैं, जिनका विषम प्रकाशिकी में अत्यधिक महत्व है। इस कार्य में मुख्य रूप से प्रभावशाली और नियंत्रित विधियाँ विकसित की गई हैं, जिनके माध्यम से विशेष प्रकाश किरणों का निर्माण, उनके गुणों का विश्लेषण और विभिन्न परिस्थितियों में उनके व्यवहार का अध्ययन किया गया है।

डैमान जालियों और स्थानिक प्रकाश अधिमिश्रक के माध्यम से चरणीय वृद्धि जैसी नवीन रणनीतियों को अपनाते हुए, नियंत्रित सूचकांक और घूमाव दिशा वाले ध्रुवण विषमता जालों को बनाए गए हैं। एक सामान्य पथ पर आधारित ध्रुवण व्यतिकरण यंत्र का उपयोग कर मिश्रित ध्रुवण भंवर बनाए गए हैं, जो सी-बिंदुओं के वलयों से घिरे होते हैं। इनकी विशेषताओं का अध्ययन स्टोक्स क्षेत्रीय विश्लेषण द्वारा किया गया है। साथ ही, एक सशक्त व्यतिकरण आधारित विधि प्रस्तुत की गई है, जिसके माध्यम से सूचकांक की समानता की पहचान कर उसे हल किया गया है। इसमें घूर्णी संवेग के दोनों भागों — आंतरिक घूर्णन और कक्षीय घूर्णन — का निर्धारण कर विषमता को स्पष्ट किया गया है। एक झुके हुए संदर्भ प्रकाश की सहायता से बने व्यतिकरण धारियों का विश्लेषण करके स्टोक्स सूचकांकों का प्रत्यक्ष निर्धारण किया गया है।

प्रकाशीय दोषों, विशेष रूप से द्विअक्षीयता (ऐस्टिग्मैटिज़्म), का प्रभाव सैद्धांतिक और प्रयोगात्मक दोनों दृष्टिकोणों से जांचा गया है। विभिन्न स्तरों की द्विअक्षीयता के प्रभाव से उत्पन्न तीव्रता वितरण के परिवर्तन का अध्ययन कर यह दिखाया गया है कि दोष और ध्रुवण संरचना के बीच एक गणनीय संबंध होता है।

यह विधि ध्रुवण विषमताओं तथा लेंस दोषों के लक्षण निर्धारण की एक नई दिशा प्रस्तुत करती है, जिसका उपयोग प्रकाशीय मापन तथा अनुकूली प्रकाशिकी में किया जा सकता है। सैद्धांतिक पूर्वानुमानों को सटीक संख्यात्मक अनुकरणों तथा नियंत्रित प्रयोगों के माध्यम से सत्यापित किया गया है, जिससे प्रस्तुत विधियों की वास्तविक उपयोगिता और सटीकता स्पष्ट होती है। यह शोध परिणाम प्रकाशीय मापन, किरण परीक्षण, कण फँसाने की विधियों तथा मुक्त माध्यम संचार तंत्रों में महत्वपूर्ण योगदान प्रदान करते हैं।

Contents

Certificate	i
Acknowledgements	ii
Abstract	iv
Contents	v
List of Figures	ix
Abbreviations	xvii
Symbols	xix
1 Introduction	1
1.1 Background and motivation	1
1.2 Optical singularities and their significance	2
1.2.1 Phase singularities	3
1.2.2 Generation of phase singularity	4
1.2.2.1 Generation of optical vortex using spiral phase plate	5
1.2.2.2 Generation of optical vortex by using spatial light modulator	6
1.2.2.3 Generation of optical vortex by using q -plate	7
1.2.3 Detection of phase singularity	7
1.3 Polarization singularities: types and characteristics	9
1.3.1 C-point singularity	10
1.3.2 V-point singularity	12
1.3.3 Generation of polarization singularities	13
1.3.4 Detection of polarization singularities	14
1.3.5 Stokes fields and Stokes phases	16

1.4	Objectives	18
1.5	Thesis organization	19
1.5.1	Chapter 1: Introduction	19
1.5.2	Chapter 2: Polarization singularity lattice generation by Dammann grating	19
1.5.3	Chapter 3: Polarization singularity lattice generation using phase ramps	20
1.5.4	Chapter 4: Polarization singularity lattice using Bessel phase engineering	21
1.5.5	Chapter 5: Detection of degenerate index states of polarization singularities by interference method.	21
1.5.6	Chapter 6: Effect of astigmatism on polarization singularities	22
1.5.7	Chapter 7: Conclusion and future scope	23
2	Polarization Singularity Lattice Generation by a Dammann Grating	25
2.1	Introduction	26
2.2	Design and implementation of Dammann grating	28
2.3	Dammann grating under spin-orbit illumination	30
2.4	Experimental realization	36
2.5	Result and discussion	38
2.6	Conclusion	41
3	Polarization Singularity Lattice Generation Using Phase Ramps	43
3.1	Introduction	44
3.2	Principles of phase ramps	46
3.3	Computational modeling of phase ramp-induced singularities	48
3.4	Experimental methods for phase ramp implementation	53
3.5	Results and discussion	55
3.6	Conclusion	60
4	Polarization Singularity Lattice Using Bessel Phase Engineering	63
4.1	Introduction	64
4.2	Phase gradients and discontinuities in Bessel beams	67
4.3	Engineering phase circulation for singularities	69
4.4	Experimental generation of composite polarization vortices	73
4.5	Results and discussion	75
4.6	Conclusion	77
5	Detection of Degenerate Index States of Polarization Singularities by Interference Method	79
5.1	Introduction	80
5.2	Degenerate index state of polarization singularities	82

5.2.1	Degeneracy	82
5.3	Fundamentals of interference in polarization singularities	83
5.4	Experimental realization for detecting degenerate states	87
5.5	Results and discussion	88
5.5.1	Spiral fringe formation	88
5.5.2	Fork fringe formation	90
5.5.3	Degenerate state identification from spiral and fork signatures	90
5.6	Conclusion	92
6	Measurement of Astigmatism using Polarization Singular beams	95
6.1	Introduction	96
6.2	Astigmatism and its mathematical representation	98
6.3	Astigmatism transformation on polarization singularity	99
6.4	Experimental setup for inducing and measuring astigmatism	105
6.5	Results and discussion	106
6.6	Conclusion	108
7	Conclusion and Scope for Future Studies	111
7.1	Summary of findings	111
7.2	Future research directions	113
	Bibliography	115
	List of Publications	131
	About the author	135

List of Figures

1.1	Images of different beam modes: the first column represents a Gaussian beam ($p = 0$), while the second and third columns depict vortex beams with topological charges $p = 1$ and $p = 2$, respectively [27].	4
1.2	Spiral phase plate	6
1.3	Schematic of the optical effect for the q -plate [33].	8
1.4	(a) and (b) show the phase patterns of the helical and tilted plane waves, respectively, while figure (c) shows the resulting intensity pattern formed due to their interference.	9
1.5	(a) and (b) Ellipse field singularity, (c) Vector field singularity	10
1.6	Illustration of the C-point singularity named as (a) lemon, (b) mon-star and (c) star singularity [49].	11
1.7	Generic V-points with polarization singularity index $\eta = \pm 1$	12
1.8	Illustration of the circular basis representation of polarization singularities. The top row showcases the intensity distributions corresponding to the scalar vortex of topological charge 1, scalar plane beam, and vector beam with a polarization singularity. Insets provide a visual representation of the phase distribution for each beam type, while the Stokes phase (ϕ_{12}) of the polarization singularity is inset in the last column of the top row. The bottom row depicts the corresponding polarization distributions for each beam type.	14
1.9	Experimental setup for measurement of Stokes parameters [56].	16
1.10	Stokes phase distributions and corresponding polarization ellipse patterns for positive and negative singularities. (a) and (c) represent the Stokes phase distribution for singularities with Stokes index $\sigma_{12} = +1$ and $\sigma_{12} = -1$, respectively. (b) and (d) shows the polarization ellipse distributions corresponding to the positive and negative singularities, illustrating the local polarization state variations.	17
2.1	Two-dimensional DG designed for generating a 2×2 spot array in diffraction.	29

2.2	Simulated 2×2 equal intensity spots produced by DG each embedded with lemon (upper panel) and star (lower panel) bright C-points (HyOPS beams) of index $I_c = \pm 1/2$. (a,d) Total intensity distribution; (b,e) Stokes phase distribution and (c,f) polarization distribution of lemon and star bright C-points. Simulation parameters of incident beams (in eqn. 5) for lemon and star lattices are ($\frac{A}{B} = 1, p = 0, q = +1, \theta_0 = 0$) and ($\frac{A}{B} = 1, p = 0, q = -1, \theta_0 = 0$) respectively.	33
2.3	Simulated 2×2 equal intensity spots produced by DG each embedded with dark C-point (HyOPS beams) of polarization index $I_c = +1$ (upper panel) and $I_c = -1$ (lower panel). (a,d) Total intensity distribution; (b,e) Stokes phase distribution and (c,f) polarization distribution dark C-points. Simulation parameters of incident beams (in eqn. 5) for $I_c = +1$ and $I_c = -1$ lattices are ($\frac{A}{B} = 1, p = -3, q = -1, \theta_0 = 0$) and ($\frac{A}{B} = 1, p = 3, q = 1, \theta_0 = 0$) respectively.	34
2.4	Simulated 2×2 equal intensity spots produced by DG each embedded with HOPS beams of polarization index $\eta = +1$ (upper panel) and $\eta = -1$ (lower panel) and represented by non-equatorial points on HOPS with coordinates (latitude = $\pi/4$, longitude = $\pi/2$). (a,d) Total intensity distribution; (b,e) Stokes phase distribution and (c,f) polarization distribution of HOPS. Simulation parameters of incident beams (in eqn. 5) for $\eta = +1$ and $\eta = -1$ lattices are ($\frac{A}{B} \approx 2.4, p = -1, q = +1, \theta_0 = \frac{\pi}{2}$) and ($\frac{A}{B} \approx 2.4, p = 1, q = -1, \theta_0 = \frac{\pi}{2}$) respectively.	35
2.5	Schematic of the experimental setup. He-Ne Laser, SF: Spatial filter, L: lenses, I: Iris, HWP: Half-wave plate, SWP: S-wave plate, SPP: Spiral phase plate, QWP: Quarter-wave plate, P: Polarizers, DG: Dammann grating, CCD: Charge-coupled device camera, PC: Computer/Laptop.	37
2.6	Experimentally obtained 2×2 equal intensity spots produced by DG each embedded with lemon (upper panel) and star (lower panel) bright C-points (HyOPS beams) of index $I_c = \pm 1/2$. (A,D) Total intensity distribution; (B,E) Stokes phase distribution and (C,F) polarization distribution of lemon and star bright C-points.	39
2.7	Experimentally obtained 2×2 equal intensity spots produced by DG each embedded with dark C-point (HyOPS beams) of polarization index $I_c = +1$ (right panel) and $I_c = -1$ (left panel). (A,D) Total intensity distribution; (B,E) Stokes phase distribution and (C,F) polarization distribution of C-points. One of the diffracted spot is taken and expanded to show the polarization distribution.	40
2.8	Experimentally obtained 2×2 equal intensity spots produced by DG each embedded with dark C-point (HyOPS beams) of polarization index $I_c = +3$ (right panel) and $I_c = -3$ (left panel). (A,D) Total intensity distribution; (B,E) Stokes phase distribution and (C,F) polarization distribution of C-points. One of the diffracted spot is taken and expanded to show the polarization distribution.	40

2.9	Experimentally obtained 2×2 equal intensity spots produced by DG each embedded with HOPS beams of polarization index $\eta = +1$ (right panel) and $\eta = -1$ (left panel) and represented by non-equatorial points on HOPS with coordinates (latitude = $\pi/4$, longitude = $\pi/2$). (A,D) Total intensity distribution; (B,E) Stokes phase distribution and (C,F) polarization distribution of HOPS. One of the diffracted spot is taken and expanded to show the polarization distribution.	41
3.1	Methods for generating OVs: (a) Three beam interference, (b) two wedge plates, (c) three wedge plates and (d) linear ramp phase variation.	47
3.2	(a) Phase for generating a linear array of vortices, (b) Simulated intensity distribution in the propagated field.	50
3.3	Two wavefronts in orthogonal states of polarization interfere to produce polarization fringes. (a) and (b) depict the phase distributions of horizontal and vertical polarized plane waves (each with different tilt) that interfere to produce polarization fringes. (c) Polarization distribution of the resultant beam. (d) azimuth contours and (e) ellipticity (polarization fringes) corresponding to the polarization distribution shown in (c). For a lemon polarization distribution shown in (f) the contours of azimuth and ellipticity are shown in (g) and (h). Fringes of any other polarization parameter can also been used to represent polarization fringes - for example in (i) contours of the Stokes parameter S_1 is drawn corresponding to the polarization distribution of (f).	51
3.4	Visualization of a simulated 2D polarization singularity lattice: Phase distribution (a) is provided to one of the polarization components (right circular polarization) to generate a polarization singular lattice (c). The lattice is embedded with generic polarization singularities of polarization index $\pm 1/2$. S_{12} Stokes phase for the lattice is depicted in (b) and one vortex is indicated by a black circle. The Stoke's phase variation around this point can be seen helical. Both (d) and (e) are zoomed versions of polarization singularities. Solid green lines are drawn to depict the orientation of the polarization singularities in the lattice. Red and blue colors represent right and left-handed polarization.	53
3.5	Schematic of the experimental setup. SF: spatial filter, L: lens, P: polarizer, HWP: half-wave plate, BS: beam splitter, SLM: spatial light modulator, QWP: quarter wave plate. (a) and (b) are the samples of phase mask display on SLM to generate lattices of polarization singularities.	54

3.6	Optical polarization lattice with singularities (a,d) are obtained experimentally by projecting phase mask (b,e) onto the SLM. Lattice is embedded with generic polarization singularities- Lemon and Star C-points. The corresponding Stokes phase S_{12} for the lattices are shown in (c,f). The solid green lines in the figures indicate the orientation of the C-points. The total intensity distribution of the lattice (a) is shown in the insets. The lattice on the right is generated by inverting the phase ramp tilt (given in (b)) in the horizontal direction. The inversion of the phase results in index inversion of polarization singularity.	56
3.7	Experimentally obtained 2D polarization singularity lattice: Polarization distributions are obtained similarly as of Fig. 3.6. In this case, the SOP of the superposing polarization components is interchanged. The interconversion of the polarization states results in the inversion of the index and handedness of polarization singularity simultaneously.	57
3.8	Experimentally obtained 2D polarization singularity lattice: Polarization distributions are obtained similarly as of Fig. 3.6. In this case, the phase mask given to SLM is divided into alternative constant and ramp phase instead of all ramped structures. The black dotted circle shows the location of C-point in Stokes phase.	58
3.9	Experimental observations of the translation and rotational motion of a polarization singularity within the lattice. Panels (a-f) illustrate the polarization distribution of the Lemon and Star C-point lattices, and (a'-f') shows the corresponding phase mask displayed on the SLM, where phase shifts are applied to alternative phase ramps, incrementally varying in steps of $\pi/3$ from 0 to 2π and are given in the top left corner of each polarization distribution.	60
4.1	Linear phase variation given by three optical components (a) Wedge plate, (b) SPP and (c) Axicon is depicted. The transverse cross-section and local phase gradient of phase distribution are given in the middle and right columns respectively for each optical component. In (b_2) and (c_2), at the centre, the gradient vector is undefined.	65
4.2	Diffraction patterns for various apertures are illustrated: (a) Circular, (b) Ring with constant phase, (c) Vortex phase, (d) and (e) Ring with vortex phase. The corresponding intensity distributions are shown in (a'), (b'), (c'), (d'), and (e') respectively.	66
4.3	Schematic showing phase discontinuity lines that exist between regions with opposite phase gradients. On the discontinuity line, two equidistant points about a specific point P on the line are out of phase. Distance $aP = Pc', bP = Pb'$ and so on. Points a and c' are out of phase. A similar feature is shared by vortex phase distribution.	68

4.4	Simulated visualization of Bessel beam phases and their corresponding intensity and polarization distributions for different orders: (a) and (b) show the Bessel beam phases of the first and second orders respectively while (c) and (d) present the engineered phases of the Bessel beams. Corresponding intensity and polarization distributions are given in the middle and bottom rows respectively. Polarization distributions are embedded with polarization vortex having polarization index $(a_2) -\frac{1}{2}$, $(b_2) -1$, $(c_2) +\frac{5}{2}$, and $(d_2) -1$ at the centre. Higher index vortex at the centre of polarization distributions (c_2) and (d_2) is also accompanied by generic singularities, lemon ($\frac{1}{2}$) and star ($-\frac{1}{2}$) C-points distributed on the rings. Rings containing polarization vortices are indicated by dashed black lines, with the polarization vortices themselves marked by solid red dots. Solid green lines represent the directrix of C-points and illustrate their orientation. Stokes phase of S_{12} Stokes field is given as inset in the upper right corner of polarization distribution in each case. (Pixel size: $6.45\mu m$, Number of pixel: 700×700)	71
4.5	Schematic of the experimental setup. SF: spatial filter, L: lens, P: polarizer, HWP: half-wave plate, BS: beam splitter, SLM: spatial light modulator, QWP: quarter wave plate. (a) and (b) are the samples of phase mask display on SLM to generate lattices of composite polarization vortices.	74
4.6	Experimental Results: Polarization vortex lattice (a), (b) and (c) are generated by projecting a phase mask, shown as inset in the upper-left corner, onto the SLM. The lattice exhibits distinctive polarization features, including generic singularities such as lemon and star C-points distributed on the rings, accompanied by a higher index vortex at the centre. Rings containing polarization vortices are indicated by dashed black lines, with the polarization vortices themselves marked by solid red dots. Solid green lines represent the directrix of C-points and illustrate their orientation. Stokes phase of S_{12} Stokes field is given as inset in the upper right corner of polarization distribution in each case.	75
4.7	Experimental observations of the translational and rotational motion of a composite polarization vortex within the lattice. Panels (a)–(f) illustrate the polarization distribution of the Lemon and Star C-point lattices. Correspondingly, panels (a')–(f') show the phase masks displayed on the SLM, where phase shifts are applied to alternate phase ramps. These shifts incrementally vary in steps of $\pi/3$ from 0 to 2π , as indicated in the top left corner of each polarization distribution.	76

5.1	Illustration of degeneracy in index, Stokes phase, and polarization for different combinations of (p, q) . The cases $(p, q) =$ (a) $(2, 1)$, (b) $(3, 2)$, (c) $(-1, -2)$, and (d) $(-2, -3)$ all result in the same index value $I_c = -\frac{1}{2}$	82
5.2	Analysis of interference fringe patterns to distinguish SAM and OAM contributions. The top row shows the interference fringe patterns corresponding to specific (p, q) combinations. The bottom row displays the fringe patterns after passing through a polarizer oriented at 45° , highlighting the shifts in fringe orientation that reveal the dominant SAM components.	86
5.3	Schematic of the experimental setup: A He-Ne Laser with wavelength 632.8nm, SF: spatial filter, L: lens, HWP: Half wave plate, PBS: Polarizing beam splitter, BS: Beam splitter, and M: mirror	87
5.4	Simulation and experimental validation of the interference patterns for C-points of polarization singular beams with different (p, q) combinations. The leftmost column shows the C-point vector fields of the beams with combinations $(1, 0)$, $(0, -1)$, $(-1, 0)$, and $(0, 1)$. The simulation results (green-dashed box) and experimental results (red-dashed box) are presented as fringe patterns under total intensity and after passing through a polarizer oriented at 45° . Changes in the position and orientation of the fork fringes confirm the SAM and OAM contributions, resolving degeneracy in the (p, q) combinations.	89
5.5	Simulation and experimental results for the interference fringe patterns of polarization singular beams with dark C-points for various (p, q) combinations: $(1, 3)$, $(-3, -1)$, $(-1, -3)$, and $(3, 1)$	91
6.1	Visualization of polarization singular beams of different index illustrating the effects of astigmatism. (a-c) represents intensity distributions, (a'-c') depict the corresponding polarization vector fields and (a''-c'') shows the resulting transformed intensity profiles.	100
6.2	Transformation of a polarization singular beam under astigmatism. (a) The initial polarization distribution with an inset showing the corresponding intensity profile. (b-d) Astigmatic phase patterns for different ratios of $\frac{a}{b}$, demonstrating the varying degrees of astigmatism. (e-g) and (h-j) Intensity distributions of the right-handed (\hat{R}) and left-handed (\hat{L}) circular polarization components, respectively, after astigmatic transformation. The orientation of the lobes, inset in each case under different astigmatic conditions.	102

6.3	Transformation of a polarization singular beam of index 1 under astigmatism. The top row (a-f) displays intensity distributions of the right-handed circularly polarized component, while the bottom row shows (a'-f') the left-handed counterpart. The degree of astigmatism is represented by the ratio $\frac{a}{b}$, with corresponding values labelled for each case. The orientation of the lobes is indicated in each image, showing the angular displacement of the singularities as astigmatism varies.	102
6.4	Transformation of a polarization singular beam with index 2 under astigmatism, resembling the behavior shown in Fig. 6.3. In this case, intensity is split into 3 lobes due to change in the index of the beam .	103
6.5	Transformation of a polarization singular beam of index 3 under astigmatism, exhibiting a pattern similar to that in Fig. 6.3. Here, the intensity splits into four lobes due to the change in the beam's index	104
6.6	Variation of the lobes' orientation difference as a function of astigmatism for polarization singular beams with indices $\eta = 1, 2$, and 3. The graph illustrates how the orientation difference increases with astigmatism.	105
6.7	Experimental setup. SF: spatial filter, L: lens, P: polarizer, HWP: half-wave plate, BS: beam splitter, SLM: spatial light modulator, QWP: quarter wave plate. (a) and (b) are the samples of the Astigmatism phase display on the SLM. (c) Schematic of astigmatic focusing with different focal lengths along orthogonal axes (f_x and f_y).	106
6.8	Experimentally obtained intensity patterns of a polarization singular beam with index $\eta = 2$ under varying degrees of astigmatism, represented by the ratio $\frac{a}{b}$. The top row (a-f) shows the orientation of the lobes for increasing astigmatism values for RCP components, while the bottom row (a'-f') presents for LCP components. The angles denote the measured orientation of the intensity lobes, demonstrating the effect of astigmatism on beam transformation.	107
6.9	Comparison of simulated and experimentally obtained lobe orientation differences as a function of astigmatism. The blue curve represents the simulated results, while the orange curve corresponds to the experimental data. The graph demonstrates a strong agreement between the two datasets, validating the experimental approach.	108

Abbreviations

PS	Poincaré Sphere
HOPS	Higher Order Poincaré Sphere
HyOPS	Hybrid Order Poincaré Sphere
PH	Poincaré Hopf
OAM	Orbital Angular Momentum
SAM	Spin Angular Momentum
SPP	Spiral Phase Plate
SLM	Spatial Light Modulator
SOP	State Of Polarization
RCP	Right Circularly Polarization
LCP	Left Circularly Polarization
HWP	Half Wave Plate
QWP	Quarter Wave Plate
PBS	Polarizing Beam Splitter
BS	Beam Splitter
SC	Stokes Camera
OV	Optical Vortex
DG	Dammann Grating
CGHs	Computer Generated Holograms

Symbols

θ	azimuthal angle
θ_0	phase shift
ϕ	phase of optical field
r	radial coordinates
I_c	C-point index
η	Poincaré-Hopf index
λ	wavelength
\hbar	reduced Planck's constant
p, q	charge of optical vortex
E	electric field
γ	azimuth of polarization ellipses
χ	ellipticity of polarization ellipses
S_0, S_1, S_2, S_3	Stokes parameters